Journal of Power Sources 265 (2014) 6–13

Contents lists available at ScienceDirect

Journal of Power Sources

journal homepage: www.elsevier.com/locate/jpowsour

Reactivity at the $Ln_2NiO_{4+\delta}$/electrolyte interface (Ln = La, Nd) studied by Electrochemical Impedance Spectroscopy and Transmission Electron Microscopy

Alejandra Montenegro-Hernández [a,b], Analía Soldati [a,b], Liliana Mogni [a,b], Horacio Troiani [a,b], Anja Schreiber [c], Flavio Soldera [d], Alberto Caneiro [a,b,*]

[a] Centro Atómico Bariloche, Av. Bustillo 9500, S.C. de Bariloche, CP 8400 Rio Negro, Argentina
[b] Consejo Nacional de Investigaciones Científicas y Técnicas (CONICET), Av. Rivadavia 1917 (C1033AAJ), Ciudad Autónoma de Buenos Aires, Argentina
[c] Helmholtz-Zentrum Potsdam, Deutsches GeoForschungsZentrum GFZ, Chemie und Physik der Geomaterialien, Telegrafenberg, C 120, D-14473 Potsdam, Germany
[d] Department of Materials Science, Saarland University, Saarbrücken, Campus D3.3, 66123 Saarbrücken, Germany

HIGHLIGHTS

- FIB-TEM study on chemical reactivity between LNO/CGO, LNO/YSZ, NNO/CGO, NNO/YSZ.
- FIB-TEM shows the beginning of the reactivity process.
- EIS suggests reactivity at $T > 600$ °C while by XRD is observed at $T > 800$ °C.
- LNO–CGO reactivity strength was higher than that of LNO–YSZ.
- The strength of NNO reactivity with YSZ and CGO was lower than that of LNO.

ARTICLE INFO

Article history:
Received 11 December 2013
Received in revised form
16 April 2014
Accepted 17 April 2014
Available online 30 April 2014

Keywords:
$Ln_2NiO_{4+\delta}$
Electrochemical Impedance Spectroscopy
Transmission Electron Microscopy-Focused Ion Beam
Chemical reactivity
Interface
Intermediate temperature-solid oxide fuel cell

ABSTRACT

Chemical reactivity between $Ln_2NiO_{4+\delta}$ (Ln: La, Nd) electrodes and $Y_{0.08}Zr_{0.92}O_{1.96}$ (YSZ) and $Ce_{0.9}Gd_{0.1}O_{1.95}$ (CGO) electrolytes was analyzed by Electrochemical Impedance Spectroscopy (EIS) and Focused Ion Beam-Transmission Electron Microscopy (FIB-TEM) techniques. $Ln_2NiO_{4+\delta}$ electrodes were deposited onto CGO and YSZ electrolytes by aerography and treated at 900 °C during 1 h in order to promote electrode adhesion. EIS spectra were collected between 500 and 800 °C in dry air. The Polarization Resistances (PR) values for La_2NiO_4/CGO/La_2NiO_4 cell are higher than those of La_2NiO_4/YSZ/La_2NiO_4. The PR for both cells and its evolution in time suggest that chemical reactivity is developed at 900 °C during the adhesion treatment and at T higher than 650 °C during the EIS measurements. The PR for Nd_2NiO_4/CGO/Nd_2NiO_4 and Nd_2NiO_4/YSZ/Nd_2NiO_4 are much lower than those of La_2NiO_4/CGO/La_2NiO_4 and La_2NiO_4/YSZ/La_2NiO_4 cells. These values and the slight increase of PR with time for Nd_2NiO_4 (NNO) electrodes indicate that the strength of chemical reactivity is much lower than that of La_2NiO_4 (LNO).

TEM results confirmed that reactivity between CGO and LNO is much higher than that of YSZ and LNO and also confirm that the strength of reactivity is appreciably lower for NNO as electrode material.

1. Introduction

Nowadays the performance improvement of Solid Oxide Fuel Cells (SOFC) and Intermediate Temperature-Solid Oxide Fuel Cells (IT-SOFC) is focused on the development of new cathode materials with high mixed conductivity, which should be thermally and chemically compatible with the other cell components. Among the mixed oxides, nickelates of composition $Ln_2NiO_{4+\delta}$ (Ln: La and Nd) are promising cathode materials due to their good transport properties [1–3] and due to the fact that they exhibit similar Thermal Expansion Coefficients (TEC) as those of conventional electrolyte materials for SOFCs and IT-SOFCs [4–6]. The crystal

* Corresponding author. Centro Atómico Bariloche, Materials Characterization, Av. Bustillo 9500, S.C. de Bariloche, CP 8400 Rio Negro, Argentina. Fax: +54 294 4445299.
E-mail address: albertocaneiro@gmail.com (A. Caneiro).

http://dx.doi.org/10.1016/j.jpowsour.2014.04.082
0378-7753/

structure of $Ln_2NiO_{4+\delta}$ consists of alternating LnO rock salt and $LnNiO_3$ perovskite layers [7,8]. This structure can accommodate extra oxygen ions in interstitial sites of the rock salt layer, generating oxygen over-stoichiometry (δ) [9,10]. The high ion mobility of these extra oxygen ions produces high ionic conductivity by interstitial oxygen diffusion [11]. However, one drawback of $Ln_2NiO_{4+\delta}$ electrodes is its reactivity with the electrolyte materials at high temperatures [2,12–14]. Since the operating temperature of the cell (500–800 °C) and the temperature of electrode/electrolyte adhesion (900 °C) are considerably high, interfacial reactivity between both components is expected. Regarding this point, Sayers et al. observed chemical reactivity between $La_2NiO_{4+\delta}$ (LNO) and $Ce_{0.9}Gd_{0.1}O_{1.95}$ (CGO) in pressed mixed powders above 800 °C [12]. Zhao et al. reported chemical reactivity between LNO and $Y_{0.08}Zr_{0.92}O_{1.96}$ (YSZ) at 1000 °C in pressed mixed powders [2] and Mauvy et al. found chemical reactivity between $Nd_{1.95}NiO_{4+\delta}$ and YSZ below 1100 °C after 4 h [13]. Recently, we observed chemical reactivity between LNO and both YSZ and CGO above 900 and 700 °C, respectively. Besides, we reported that $Nd_2NiO_{4+\delta}$ (NNO) at 1000 °C reacts with both YSZ and CGO in mixed powders after 2 h and 72 h of treatment, respectively [14]. In all of these tests, XRD was used to detect reactivity.

In order to better understand the performance of the SOFC cells, it is necessary to study the cathode/electrolyte interface. This is especially important in cases such these presented here, where reaction between the main cell components is expected at the operation temperatures. Electrochemical Impedance Spectroscopy (EIS) is one of the main tools used to characterize interfacial phenomena [15,16]. This technique allows identifying the limiting process for oxygen reduction among various reaction steps which are normally related to the electrode and surroundings, such as the electrode/electrolyte contact area [17] and the interface integrity [18]. On the other hand, TEM is a powerful tool to study sample's features such as local chemical composition, crystalline nature, micro and nano-structure of the cell components such as electrode, electrolyte and electrode/electrolyte interface even at atomic resolution [19].

TEM is a technique that requires very thin samples (<100 nm thickness) to allow electrons to transmit through the material with enough intensity. However, the electrode/electrolyte interface in an SOFC is a zone where two phases with different composition, grain size, density, porosity, mechanical and chemical characteristics coexist. Therefore, a TEM preparation method which involves physical abrasion or electrochemical polishing is not suitable, since each phase can be affected differently. For this kind of samples FIB is the most appropriate preparation technique [20]. A Scanning Electronic Microscope (SEM) coupled to FIB facilitates the precise site selection and the thinning is performed with a Ga-ions gun installed in the same chamber (SEM-FIB) [21].

In this work we analyzed the chemical reactivity effect on the electrode/electrolyte interfaces monitoring the evolution of Polarization Resistance (PR) over time by EIS. After completing EIS measurements, the interfaces were characterized by FIB-TEM and Energy Dispersive Spectroscopy (EDS). Possible artifacts from the FIB preparation method were also evaluated.

2. Experimental

2.1. Samples preparation

The lanthanide nickelates, LNO and NNO powders, were synthesized by HMTA (hexamethylenetetramine) method [14,22], using analytic grade La_2O_3, Nd_2O_3 and $Ni(CH_3COO)_2{\cdot}H_2O$ as precursors. Stoichiometric amounts of precursors were dissolved in acetic acid with HMTA and acetylacetone, in a (ligand:metal) 3:1 M ratio. The solution was refluxed and heated until a brown gel was obtained. This gel was fired at 400 °C and finally annealed at 950 °C.

Symmetrical electrode/electrolyte/electrode cells were conformed depositing by aerography on both sides of a dense YSZ or CGO electrolyte, a slurry containing a fine powder of $Ln_2NiO_{4+\delta}$ (Ln = La and Nd) cathode material. The dense electrolyte was obtained by pressing fine powder of CGO or YSZ under a pressure of 75 kg cm^{-2} and sintering at 1350 °C for 4 h $Ln_2NiO_{4+\delta}$ slurry was prepared by mixing $Ln_2NiO_{4+\delta}$ powders with ethanol, α-terpineol, polyvinyl butyral, and polyvinylpyrrolidone in a 40:30:27:2:1 ratio. After slurry deposition, the symmetrical assemblies were heat treated at 900 °C for 1 h to promote electrode/electrolyte adhesion. Electrode porous film's thickness evaluated by SEM was approximately 10 μm.

2.2. Samples characterization

The EIS technique was used to characterize the oxygen reduction reaction in $Ln_2NiO_{4+\delta}$ cathodes. These measurements were performed with a frequency response analyzer (FRA) coupled to an AUTOLAB potentiostat, operating within 500–800 °C temperature range, under synthetic air flow (Ar_2-20 % O_2). In this work Au mesh was chosen as current collector for EIS experiments since chemical reactivity between Pt and Ln_2NiO_4 at high temperatures has been previously reported [23–25]. The EIS measurements were performed each 50 °C by increasing T from 500 to 800 °C. At each selected temperature the dwell period was approximately 60 h.

After 400 h, the total period of the EIS measurements, the pellets were broken into pieces and mounted in an SEM sample holder, with the cathode side upwards. FIB was used as site specific sample preparation method for TEM measurements. Two instruments were used: An FEI-FIB 200 at the Geo-Forschungs-Zentrum Potsdam (Germany) and a Helios NanoLab 600 Dual beam (SEM/FIB) system (FEI) at the Saarland University (Germany). A Pt layer of 200 nm thickness and 15 μm length was first deposited on cathode surfaces by using the electron beam, covering selected areas to protect the underlying material from the sputtering process. Further Pt was deposited with the ion beam achieving a thickness of about 1 μm. The Ga-ion beam at 30 kV was used to remove material on both sides of Pt layer. In this way lamellas of 15 × 10 × 0.15 μm^3 were obtained. Some of the lamellas were further thinned with the ion beam, with a final voltage of 5 kV in order to evaluate possible artifacts due to the FIB preparation. The lamellas were afterward lift-out transferred to a Cu TEM grid by using a micromanipulator. The TEM instruments used for this study were a Philips CM 200 UT equipped with an EDAX-EDS analyzer and a TECNAI F20 FEG TEM–STEM microscope equipped with an HAADF detector and EDAX-EDS analyzer. EDS line-scan were performed each 5 nm using a spot size of 2 nm and a dwell time of 5 s. The concentration values were determined through the Cliff-Lorimer ratio technique using the EDAX-TEAM software. Ce, Zr, Y, Gd, La and Nd concentrations were calculated with the L- and Ni with the K-emissions respectively. The signal was processed using an average smoothing with a 5 points window.

3. Results and discussion

3.1. LNO/YSZ and LNO/CGO interfaces

Fig. 1 shows the variation of the LNO Area Specific Resistance (ASR) with time at 650, 700 and 750 °C using YSZ (left column) and CGO (right column) as electrolytes. The ASR is computed by the relation ASR = PR * A/2, where PR is the Polarization Resistance and A is the cathode geometric area [26]. It can be observed that the ASR of LNO/YSZ/LNO at 650 °C and at 700 °C decreases with time, and

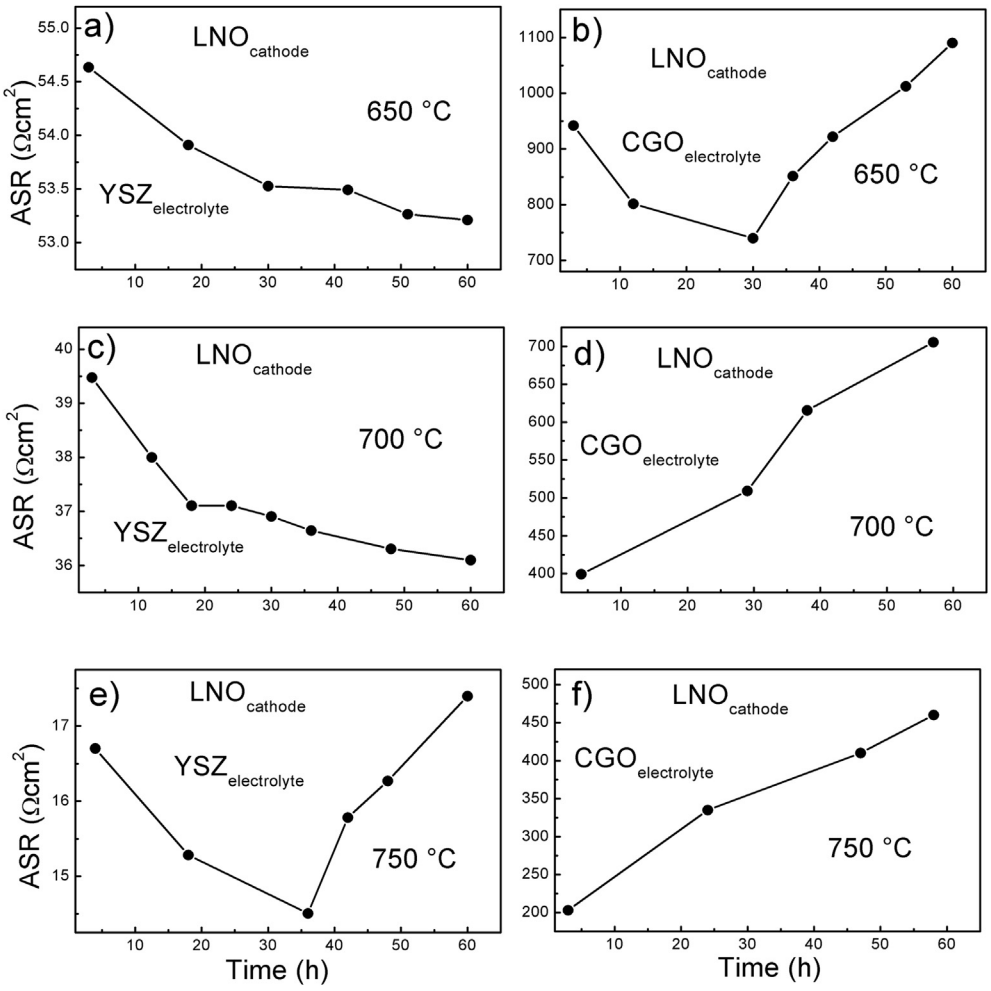

Fig. 1. ASR values as function of time at 650, 700 and 750 °C for LNO/YSZ/LNO and LNO/CGO/LNO cells.

for LNO/YSZ/LNO at 750 °C and LNO/CGO/LNO at 650 °C ASR decreases showing a minimum up to ∼30–35 h and then increases for larger times. For LNO/CGO/LNO at 700 °C and 750 °C the ASR always increases. The ASR values of the symmetrical cells with CGO as electrolyte are approximately 20 times higher than those of cells with YSZ as electrolytes for the three temperatures monitored in this study. The origin of the ASR decrease with time is not evident. However, as speculation, this effect could be associated to a mechanical relaxation of the Au grid at these temperatures, thus increasing the Au/LNO contact points numbers. This mechanical relaxation takes more time when the temperature is lower, and is more significant at 650 °C and 700 °C than at 750 °C. The difference on the magnitude of the ASR decrease between LNO/YSZ/LNO and LNO/CGO/LNO cells could be due to a different mechanical pressure performed on the Au grids of each cell. However, a competition between this mechanical relaxation and reactivity seems to be present. In the case of cells with CGO as electrolyte the reactivity is much higher and a decrease of ASR due to the mechanical relaxation of the Au grid is evident at lower temperatures ($T \leq 650$ °C). After this event, a continuous increase of ASR with time as shown in Fig. 1b), d), e) and f) should be associated to a different effect.

Lee et al. studied the $La_{0.9}Sr_{O.1}MnO_3$/YSZ/$La_{0.9}Sr_{O.1}MnO_3$ cell and determined that the increase in the resistance value is due to the formation of $La_2Zr_2O_7$ at the electrode/electrolyte interface [27]. The presence of this compound induces resistive losses, because of its poor electrical transport properties. In a similar manner, the

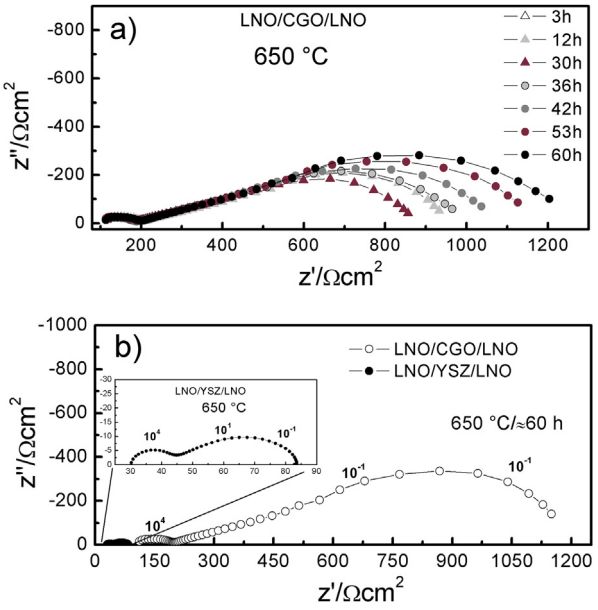

Fig. 2. a) EIS spectra in air at 650 °C for LNO/CGO/LNO cell collected at different periods of time. b) Comparison of EIS spectra between LNO/CGO/LNO and LNO/YSZ/LNO cells collected in air at 650 °C after 60 h.

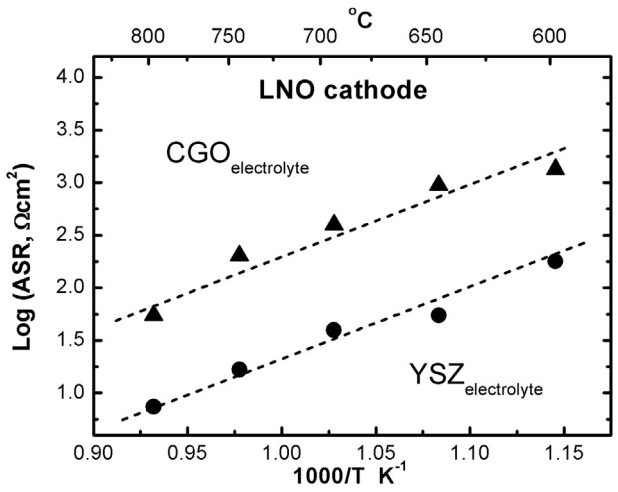

Fig. 3. ASR and its dependence with temperature for LNO/YSZ/LNO and LNO/CGO/LNO cells.

increase on the ASR values observed in our LNO/YSZ/LNO and LNO/CGO/LNO cells should be caused by reactivity at the electrode/electrolyte interface similarly to that observed by Lee et al. It should be pointed out that the reactivity suggested by the increase of ASR, may occur not only due to the long periods at high temperatures imposed by the EIS measurement itself, but also due to the electrode/electrolyte adhesion treatments, which were carried out at 900 °C during 1 h [14,23].

In Fig. 2 are shown two representative EIS spectra in the Nyquist representation. One of them corresponds to the Nyquist plot of LNO/CGO at 650 °C as function of time and the other one shows a comparison between LNO/YSZ and LNO/CGO at 650 °C after 60 h.

According to a previous work [24] the impedance spectra consists of three contributions: a high frequency attributed to oxygen ion transfer from the electrode to the electrolyte, a medium frequency range assigned to oxygen ion diffusion co-limited by charge transfer, and a low frequency region due to dissociated absorption.

Fig. 3 compares the ASR values vs. temperature for LNO/YSZ/LNO and LNO/CGO/LNO cells. The ASR values plotted in this figure correspond to those measured at the beginning of dwell time at each temperature ($t < 5$ h). These values for $T = 650$, 700 and 750 °C correspond to the first points shown in Fig. 1a)–f). The ASR is higher for the LNO/CGO/LNO cell. Therefore, this fact suggests that the effect of reactivity occurring at 900 °C during the adhesion treatment is much higher for CGO as electrolyte.

FIB-TEM and STEM studies were carried out after EIS measurements with the aim of observing microstructural changes occurring at the electrode/electrolyte interface as a consequence of reactivity.

Fig. 4 shows a bright field TEM image of the LNO/YSZ interface. In some places the presence of an interfacial compound is detected (named "reaction layer") which is also extended between LNO grains (Fig. 4a)), affecting both, the triple phase boundary (TPB) and the cathode surface. Magnification of the interfacial region is shown in Fig. 4b); the reaction layer presents a very different microstructure than those of LNO or the YSZ bulk phases. In Fig. 4c) an STEM-HAADF image of the reaction zone where an LNO grain, a reaction layer and YSZ grain are shown. The arrow indicates the line and direction of the line-scan (300 nm). On one hand, the La

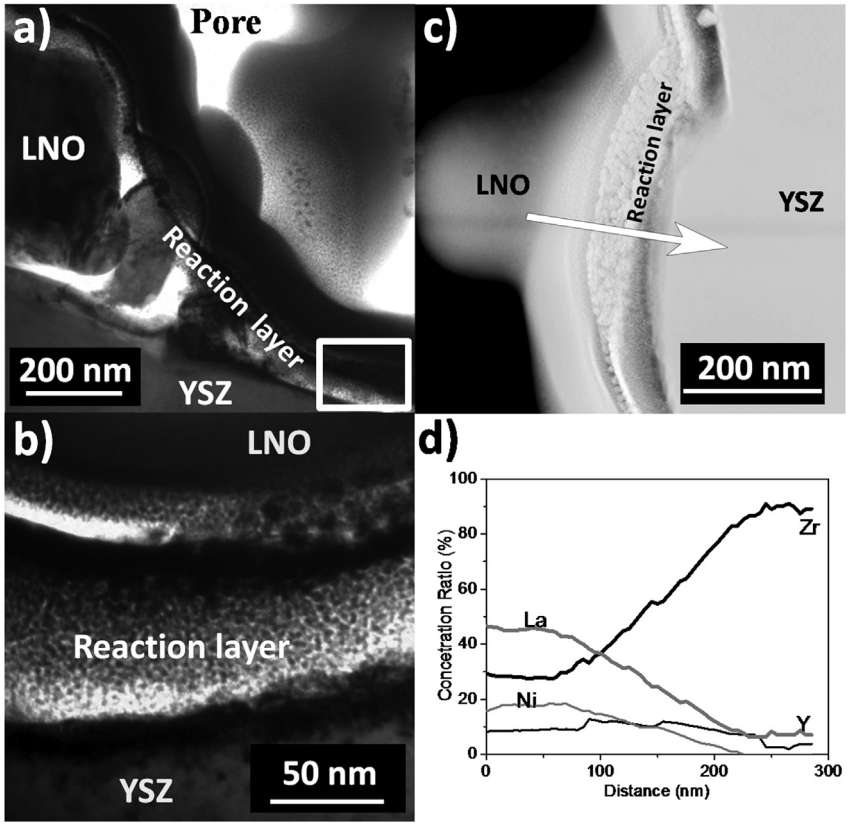

Fig. 4. a) Bright field TEM image of the interfacial zone of an LNO/YSZ lamella after EIS measurements. b) Magnification of the inset shown in a) where sings of a chemical reaction between both phases are observed. c) STEM image of a reaction zone at the LNO/YSZ interface collected with an HAADF detector. d) La, Ni, Y and Zr concentrations profiles along the line-scan indicated by the arrow of c).

concentration decreases in the direction of the arrow and goes to zero in the electrolyte region. On the other hand, Zr is present in the reacted LNO grain and increases its concentration in the reaction layer. It is worth to observe that La and Zr concentrations are similar in the reaction layer, which suggest the formation of the insulator pyrochlore $La_2Zr_2O_7$ phase. The Ni concentration profile is similar to that of La.

These analyses indicate that the increment of the ASR value may be caused by: (1) a degradation of LNO bulk cathode material close to the LNO/YSZ interface (see Fig. 4a)) and (2) the growth of a high-resistive interfacial compound.

The LNO/CGO interface was also studied by FIB-TEM and STEM. Fig. 5 shows the results of these analyses.

A bright field TEM image of the LNO/CGO lamella is presented in Fig. 5a). The cathode/electrolyte interface is marked with a double arrow. Inside the cathode zone the presence of pores is observed (light or white regions, marked with a single arrow), and also a material surrounding the particles of LNO (light gray regions). The contrast of this material clearly differs from the LNO, CGO and pores, and it is widely distributed in the cathode, while it is not present in the electrolyte. The Electron Diffraction pattern is shown in Fig. 5b). The pattern shows only a diffuse ring, which is characteristic of an amorphous material [28]. In Fig. 5c) it is displayed an STEM image collected with an HAADF detector where small grains of the electrode, grains of the electrolyte and the amorphous reaction region are observed. The EDS analysis was performed scanning a line of 550 nm length. In Fig. 5d) are plotted the Ce, La, Ni and Gd concentrations along the line. Ce is detected in the grain of the electrode which may be due to the presence of reacted amorphous material below the electrode grain. In addition, Ce is the main element present in the amorphous material. An EDS analysis of high statistic (50 s) in the amorphous region (not showed) detected the presence of Ce as majority element and Ni and Gd as minority elements. Furthermore, it was found that the composition of this amorphous compound is similar in different regions of the cathode. The peaks of La and Ni observed at 350 nm of the line-scan indicate the formation of a reaction layer containing mainly Ce and La. This region appears with a brighter contrast in the HAADF image suggesting a higher *Z* average. Clearly, the formation of the amorphous material at the cathode/electrolyte interface and at the cathode bulk material is related to chemical reactivity between CGO and LNO. It is assumed that chemical reaction begins at the interfacial region and after it extends beyond the cathode. These results would explain the high ASR values obtained for LNO/CGO/LNO cells as compared with those of LNO/YSZ/LNO cell, where the reactivity region is located close to the electrolyte/electrode interface. In this case an insulator layer formed at the interface increases the ASR. On the other hand, for LNO/CGO reactivity between both compounds affects not only the interface but also the electrode grains in a region of few microns (see Fig. 5a)).

3.2. NNO/YSZ and NNO/CGO interfaces

EIS measurements for NNO/YSZ/NNO and NNO/CGO/NNO cells vs. time were performed at 700 °C in air. EIS measurements at temperatures lower than 700 °C are not shown since ASR values remain practically unchanged during periods as long as 24 h.

Fig. 6 shows the ASR values as a function of time for NNO/YSZ/NNO and NNO/CGO/NNO cells at 700 °C operating temperature. The ASR values obtained for the two cells present a slight increase with time, which do not exceed 10 %. The ASR values for NNO/CGO/NNO and NNO/YSZ/NNO cells are similar between them and are lower than those obtained with LNO as electrode and CGO as

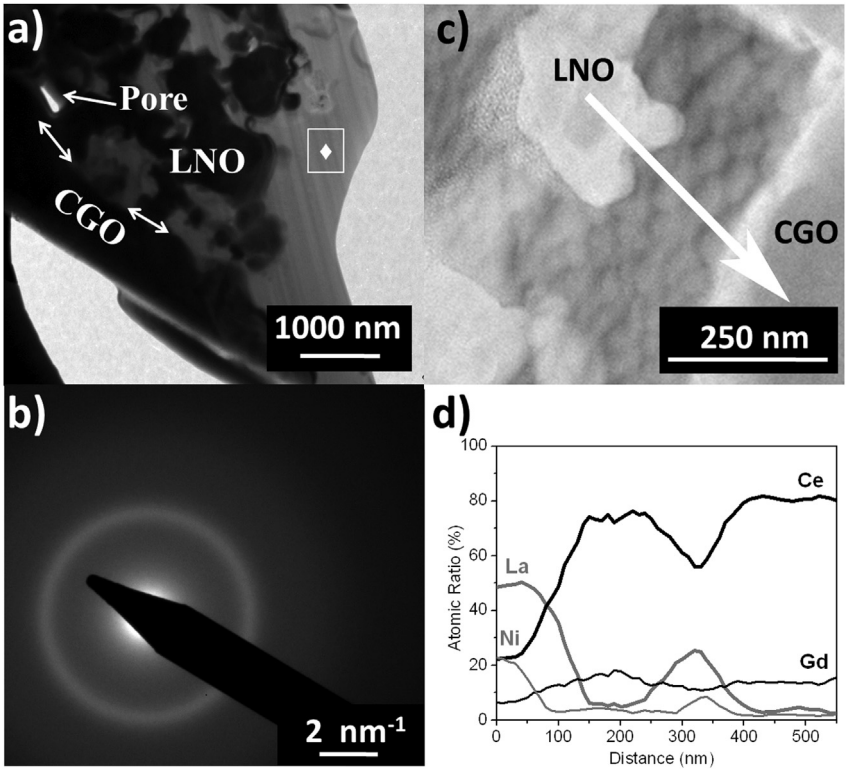

Fig. 5. a) Bright field TEM image of the chemical reaction zone in an LNO/CGO lamella after EIS measurements. b) Electron diffraction pattern of a zone with sings of chemical reaction (◆), c) STEM image of a reaction zone at the LNO/YSZ interface collected with an HAADF detector. d) La, Ni, Ce and Gd concentrations profiles along the line-scan indicated by the arrow of c).

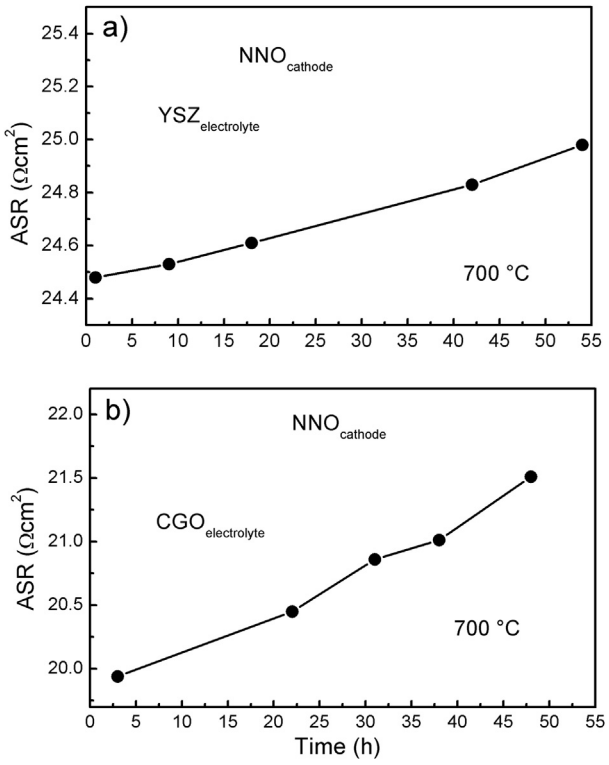

Fig. 6. ASR values as function of time for NNO/YSZ/NNO and NNO/CGO/NNO cells.

electrolyte. In these measurements a decrease of the ASR with time at the beginning of the operating time was not observed.

The slight increase of the ASR suggests also reactivity at the NNO/CGO and NNO/YSZ interfaces, but this reactivity should be much lower than that occurring at the LNO/CGO and LNO/YSZ interfaces. This effect is expected because the strength of chemical reactivity for NNO/YSZ and NNO/CGO is much lower than that of LNO/YSZ and LNO/CGO as previously reported through XRD analysis [14].

Fig. 7a) shows an STEM-HAADF image of the NNO/YSZ interface where a YSZ grain, a brighter reaction layer, an intermediate reaction zone, and an NNO grain can be observed. In Fig. 7b) are plotted the concentration of Zr, Nd, Y and Ni along the EDS line-scan. The scan was performed on a length of 400 nm. The Zr concentration is depleted while that of Nd shows a peak in the brighter region layer indicating reactivity. Zr, Y, Nd and Ni in a low concentration are present in the intermediate reaction zone. Zr and Y concentrations decrease while Nd and Ni concentrations increase in the border of NNO grain.

For NNO/CGO (Fig. 7c) and d)) the STEM-HAADF image shows a small reacted grain (NNO) containing Nd, Ni and Ce, a reaction layer and the CGO electrolyte. In Fig. 7d) are plotted the concentration of Ce, Nd, Gd and Ni along the EDS line-scan. The scan was performed on a length of 350 nm. The reaction layer contains mainly Nd and Ce and Ni as minority element. This profile indicates that Ce diffuses into the NNO and Nd should diffuse in CGO. The compound formed due to reactivity could correspond to the $Ce_{1-x}Nd_xO_{2-x/2}$ fluorite phase [14,24].

Chemical reactivity between NNO and both YSZ and CGO is present at 700 °C and even at lower temperatures, for prolonged annealing times. However, the comparison of the ASR values between LNO/CGO/LNO and NNO/CGO/NNO cells and the TEM bright field images between LNO/CGO and NNO/CGO interfaces clearly show that reactivity is considerably lower for NNO/CGO.

The present results obtained by EIS and FIB-TEM show that these techniques can resolve the beginning of the reactivity process while the usual XRD reactivity test [14] detects reactivity in a more advance stage.

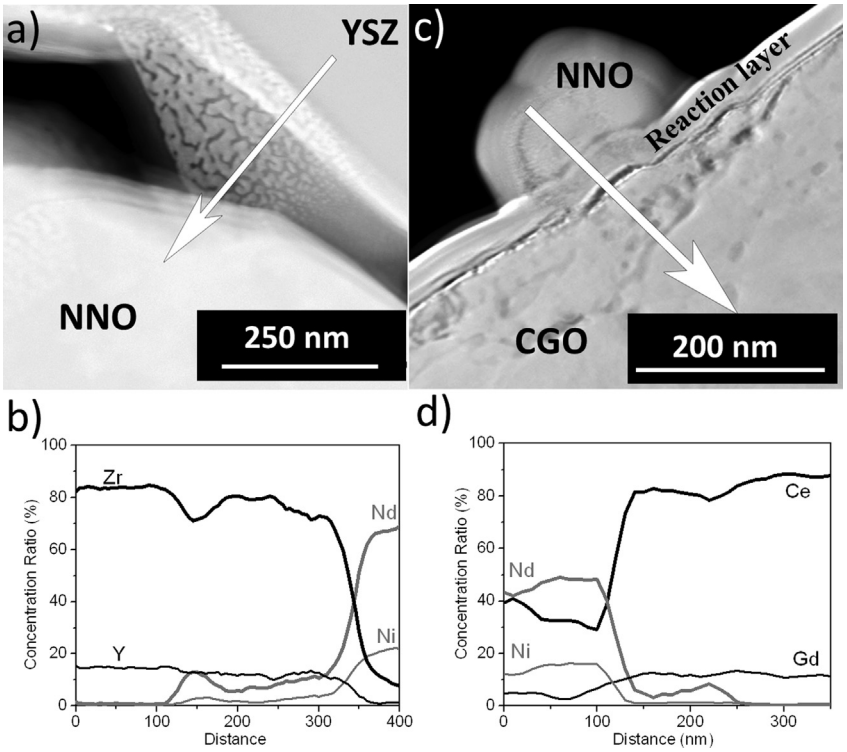

Fig. 7. STEM images of interfacial zones of NNO/YSZ a) and NNO/CGO c) lamellas obtained by FIB, after EIS measurements. b) Nd, Ni, Zr and Y concentrations profiles along the line-scan indicated by the arrow of a). d) Nd, Ni, Ce and Gd concentrations profiles along the line-scan indicated by the arrow of c).

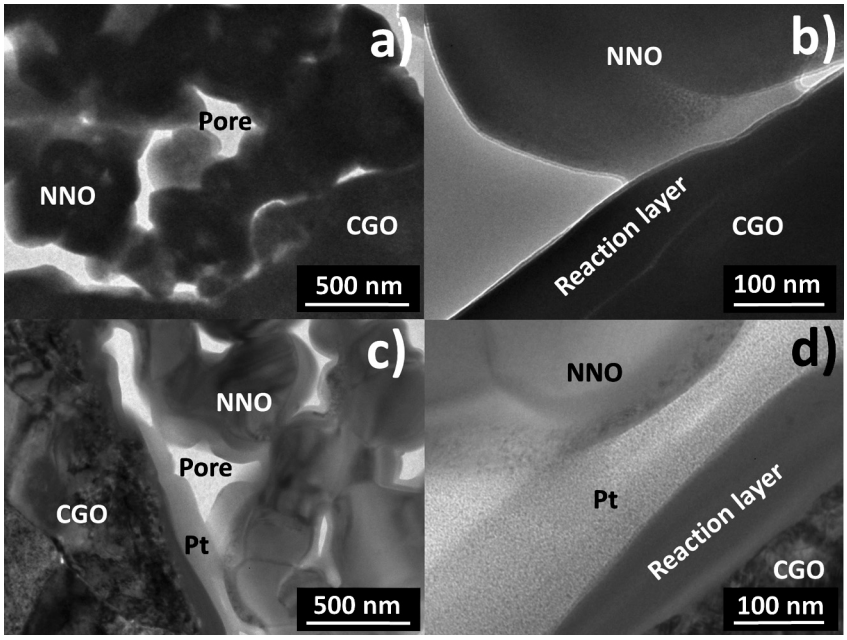

Fig. 8. Bright field TEM images of interfacial zones of NNO/CGO lamella. a) and b) lamella prepared by conventional way and c) and d) lamella further thinner after fill the material pores with Pt.

3.3. Evaluation of secondary effects caused by preparation of the TEM samples by FIB

FIB is a powerful technique to prepare thin lamellas for TEM. However, an open question is if the observed regions, particularly the reaction zone, is a characteristic of the sample or corresponds to amorphization or redeposition of the material removed by the ion beam. In order to prove this, a final essay was performed. The NNO/CGO interface was selected for this essay due to its low reactivity. The essay consists of filling the cathode pores of a thick lamella (200 nm) with Pt using the electron beam, after the lift out process. The filling of the pores with platinum improves the mechanical integrity of the lamella. After that, the lamella was thinned again (to ~80 nm) by FIB but using ions of lower energy. This procedure allows obtaining thinner lamellas than those obtained without Pt filling.

Fig. 8 shows a comparison of TEM images of a lamella as-prepared (a) and b)) with a lamella thinned after Pt incorporation (c) and d)).

Comparing TEM images it can be seen that, as expected, the lamella obtained by incorporation of Pt is thinner and allows better transmission signal. In both samples the reaction layer is located on the CGO surface and the morphologies and thickness of this layer are similar. On the other hand, this layer is not observed on the NNO bulk grains (which are not in contact with the electrolyte) and also not filling the cathode pores. From these observations we conclude that the layer (marked as "reaction layer" in Fig. 8b) and d)) on the CGO grains corresponds to a reaction between CGO and NNO and is not due to a secondary effect of material re-deposited caused by the FIB preparation.

3.4. General remarks

The characterization of the electrode/electrolyte interface and its evolution with time is essential to understand the performance of electrochemical devices operating at high temperatures such as IT-SOFC and SOFC. When reactivity between electrode and electrolyte materials is present, thermal activated processes such as diffusion operate and their effect increases with temperature, leading to the formation of other compounds at the electrode/electrolyte interface. The effect of this reactivity is reflected as a continuous spoilage of the cell performance.

Considering the thermal activated nature of the diffusion process, the operation temperature of the high temperature electrochemical devices should be enough low as compared to the temperature at which reactivity takes place. Thus, if reactivity is developed over time, its effect should be not significant, at least during the lifetime of the SOFC and IT-SOFC. One case in which this seems to happen was well illustrated for cobaltites electrodes of composition $La_{0.4}Sr_{0.6}Co_{0.8}Fe_{0.2}O_{3-x}$ (LSCF) deposited onto CGO electrolyte [19,29]. An FIB-TEM study similar to the present one showed the presence of a semi-coherent interface between LSFC and CGO after a thermal treatment of 1000 h at 500 °C. Neither the presence of reactivity nor evolution of the ASR with time was detected at this operation temperature. From this example one might conclude that a desirable interface should be that in which both the electrode and electrolyte crystalline structures are related in such way that allows the formation of coherence or semi-coherence. This feature may help the transfer of oxygen ions between electrode and electrolyte.

Reactivity affects not only the electrode/electrolyte interface but also the Triple Phase Boundary (TPB) and the active surface of the electrode exposed to the gas atmosphere. The electrode reaction at the cathode for a mixed conductor involves different steps such as oxygen diffusion in the gas phase, dissociation of molecular O_2 at the surface of the electrode, incorporation of the oxygen to the electrode, diffusion of the oxygen ions within the electrode and transfer of the oxygen ions from the electrode to the electrolyte [29]. Each step depends on the particular features of the electrode microstructure. Thus, the presence of reactivity which modifies the electrode microstructure could change the relative weight of the different steps. This has been recently observed for NNO/CGO/NNO cells where reactivity affects mostly electrodes of small particle size [24]. Thus, the ratio between reacted and unreacted zones is larger for smaller grains [24]. The consequence of this is a modification of the limiting step of the electrode reaction.

The use of TEM/STEM with lamellas prepared by FIB allows a direct observation of the electrode/electrolyte interface with a great detail making this technique a powerful tool for studying the causes of aging of electrochemical devices operating at high temperatures.

4. Conclusions

The effect of chemical reactivity at the cathode/electrolyte interface on the ASR values was studied by the EIS technique following the ASR evolution with time, at different temperatures. The microstructure of the cathode at the electrode/electrolyte interface was studied by TEM/STEM in FIB prepared samples. Combining both techniques it was possible to understand the origin of the degradation of nickelates cathodes onto two different electrolytes YSZ and CGO.

These studies suggest that $La_2Zr_2O_7$ could be present at the LNO/YSZ interface. The formation of this compound due to chemical reaction between LNO and YSZ is the cause of a continuous increment of ASR values with time for LNO cathode. By comparing the EIS spectra of LNO/CGO/LNO with LNO/YSZ/LNO cells, it can be seen that ASR values for LNO/CGO cell are much higher than those determined for the LNO/YSZ cell. This fact suggests that the strength of reactivity between LNO-CGO is higher than that of LNO–YSZ. As it could be observed by analyzing the LNO/CGO interface by TEM, an amorphous material was formed at the interface and surrounding the cathode. This could indicate that reactivity begins at the interfacial zone and then extends beyond this region. These results show that reactivity is a drawback for the use of LNO as cathode material for IT-SOFC and SOFC cells using CGO or YSZ as electrolyte. At least when the operating temperature is higher than 650 °C.

In contrast to the test performed by XRD which does not indicate reactivity between NNO with YSZ and CGO [14,24] at T below 1000 °C, both EIS and FIB-TEM results, show chemical reactivity at lower temperatures, namely from $T = 700$ °C. The reactivity occurs during the adhesion treatment for 1 h at 900 °C and even at 700 °C during the EIS measurements as shown by the increase of ASR with time. However, the increment of the ASR with time for both cells was less than 10 % over a period of 50 h. Then, the strength of chemical reactivity for NNO/CGO/NNO, NNO/YSZ/NNO is much lower than that of LNO/YSZ/LNO and LNO/CGO/LNO cells. The preparation of lamellas by FIB and observed by TEM/STEM allows to confirm evidences of reactivity suggested from a highly sensitive interfacial technique such as EIS.

Acknowledgments

This work was financially supported by Comisión Nacional de Energía Atómica (CNEA), Consejo Nacional de Investigaciones Científicas y Técnicas (CONICET Grant PIP 11220110100366CO), Universidad Nacional de Cuyo (UNCuyo) and Agencia Nacional de Promoción Científica y Tecnológica (ANPCyT Grant PICT2010-0322). F.S. thanks the EFRE Funds of the European Commission for support of activities within the AME-Lab project. The authors kindly thank Dr Adriana Condó and Mr Adriano Geracci from the Metals Department of Centro Atómico Bariloche for their valuable support with the STEM analyses.

References

[1] J.M. Bassat, P. Odier, A. Villesuzanne, C. Marin, M. Pouchard, Solid State Ionics 167 (2004) 341–347.
[2] H. Zhao, F. Mauvy, C. Lalanne, J. Bassat, S. Fourcade, J. Grenier, Solid State Ionics 179 (2008) 2000–2005.
[3] E. Boehm, J. Bassat, P. Dordor, F. Mauvy, J. Grenier, P. Stevens, Solid State Ionics 176 (2005) 2717–2725.
[4] V.V. Kharton, A.P. Viskup, A.V. Kovalevsky, E.N. Naumovich, Solid State Ionics 143 (2001) 337–353.
[5] L. Minervini, R.W. Grimes, J.A. Kilner, K.E. Sickafus, J. Mater. Chem. 10 (2000) 2349–2354.
[6] S.J. Skinner, J.A. Kilner, Solid State Ionics 135 (2000) 709–712.
[7] E.N. Naumovich, M.V. Patrakeev, V.V. Kharton, A.A. Yaremchenko, D.I. Logvinovich, Solid State Sci. 7 (2005) 1353–1362.
[8] S.J. Skinner, Solid State Sci. 5 (2003) 419–426.
[9] M.T. Fernández-Díaz, J.L. Martinez, Solid State Ionics 63–65 (1993) 902–906.
[10] K. Ishikawa, W. Shibata, K. Watanabe, T. Isonaga, M. Hashimoto, Y. Suzuki, et al., J. Solid State Chem. 131 (1997) 275–281.
[11] V.V. Vashook, I.I. Yushkevich, L.V. Kokhanovsky, L.V. Makhnach, S.P. Tolochko, I.F. Kononyuk, et al., Solid State Ionics 119 (1999) 23–30.
[12] R. Sayers, J. Liu, B. Rustumji, S.J. Skinner, Fuel Cells 8 (2008) 338–343.
[13] F. Mauvy, C. Lalanne, J. Bassat, J. Grenier, H. Zhao, P. Dordor, et al., J. Eur. Ceram. Soc. 25 (2005) 2669–2672.
[14] A. Montenegro-Hernández, J. Vega-Castillo, L. Mogni, A. Caneiro, Int. J. Hydrogen Energy 36 (2011) 15704–15714.
[15] B.-K. Lee, J.-Y. Lee, H.-Y. Jung, J.-H. Lee, J.-H. Hwang, Solid State Ionics 179 (2008) 955–959.
[16] D.E. Vladikova, Z.B. Stoynov, A. Barbucci, M. Viviani, P. Carpanese, J.A. Kilner, et al., Electrochim. Acta 53 (2008) 7491–7499.
[17] J. Nielsen, M. Mogensen, Solid State Ionics 189 (2011) 74–81.
[18] A. Chen, J.R. Smith, K.L. Duncan, R.T. DeHoff, K.S. Jones, E.D. Wachsman, J. Electrochem. Soc. 157 (2010) B1624.
[19] A.L. Soldati, L. Baqué, H. Troiani, C. Cotaro, A. Schreiber, A. Caneiro, et al., Int. J. Hydrogen Energy 36 (2011) 9180–9188.
[20] L.A. Giannuzzi, F.A. Stevie, Micron 30 (1999) 197–204.
[21] R. Wirth, Chem. Geol. 261 (2009) 217–229.
[22] L. Baque, E. Djurado, C. Rossignol, D. Marinha, A. Caneiro, A. Serquis, Electrochem. Soc. 25 (2009) 2473–2480.
[23] A. Montenegro-Hernández, L. Mogni, A. Caneiro, Int. J. Hydrogen Energy 35 (2010) 6031–6036.
[24] A. Montenegro-Hernández, L. Mogni, A. Caneiro, Int. J. Hydrogen Energy 37 (2012) 18290–18301.
[25] R. Sayers, S.J. Skinner, J. Mater. Chem. 21 (2011) 414.
[26] C. Déportes, M. Dudot, P. Fabry, J. Fouletier, A. Hammou, M. Kleitz, E. Siebert, J.-L. Souquet, Electrochimie des Solides, Press Universitaires de Grenoble, Grenoble, 1994.
[27] H.Y. Lee, S.M. Oh, Solid State Ionics 90 (1996) 133–140.
[28] D.B.B. Williams, C.B. Carter, Transmission Electron Microscopy: A Textbook for Materials Science, Plenum Press, New York, 1996.
[29] S.B. Adler, Chem. Rev. 104 (2004) 4791–4843.